 https://doi.org/10.3311/PPch.19673
Creative Commons Attribution

Periodica Polytechnica Chemical Engineering, 66(3), pp. 494–502, 2022

Evolved Gases and Unified Kinetic Model for Low-temperature Thermal Decomposition of Rice Straw Hydrolysis Residue for Possible Value Addition

Himadri Roy Ghatak[1*]

[1] Department of Chemical Engineering, Sant Longowal Institute of Engineering and Technology, Longowal 148106, Punjab, India
[*] Corresponding author, e-mail: hrghatak@sliet.ac.in

Received: 09 December 2021, Accepted: 30 March 2022, Published online: 11 May 2022

Abstract

Low-temperature thermal decomposition (LTTD) of Rice straw hydrolysis residue (RSHR) was studied using thermogravimetric analysis and Fourier Transform Infrared spectroscopy (TGA-FTIR) at different heating rates. During thermogravimetry, the maximum rate of mass loss of 135% per min was observed at 339 °C (T_{max}) for heating rate of 50 °C per min. T_{max} decreased to 323, 315, and 299 °C with decrease in heating rate to 40, 30, and 20 °C min^{-1}, respectively. LTTD of RSHR yields volatile oxygenated organics – acids, esters, aldehydes, ketones, alcohols and phenols – as revealed by the FTIR spectra of evolved gases. At increased decomposition temperature, carbonyl moieties were less conjugated. The main gaseous products of LTTD were carbon dioxide, carbon monoxide, and methane. Kinetics of LTTD of RSHR was analysed using thermogravimetry results. Activation energy of LTTD followed a Lorentzian distribution with respect to residual mass fraction (RMF). Dependence of LTTD rate on RMF was found to adhere to the truncated Sestak and Berggren model.

Keywords

rice straw hydrolysis residue, low-temperature thermal decomposition, TGA-FTIR, activation energy, evolved gases

1 Introduction

On one hand, managing the agricultural residue from food grain cultivation is a big challenge in India. The current practice of large scale burning of rice straw in the field is associated with colossal environmental implications and the loss of precious renewable resource [1, 2]. On the other hand, our country faces the challenge of reducing its dependence on fossils for its energy needs [3]. Production of 2nd generation bioethanol is one possible alternative to manage this waste and there is special thrust on this in the National Policy on Biofuels [4]. In all 12 lignocellulosic biorefineries are planned at estimated investment of USD 1.4 billion (INR 10 billion). Govt. of India has ambitious investment plans to promote this in the coming years through Viability Gap Funding to the tune of USD 0.7 billion (INR 50 billion) [4]. Production of bioethanol from lignocelluloses targets the carbohydrate fraction. Among several methods, acid hydrolysis remains a method of choice for obtaining fermentable sugars from the carbohydrate fraction of the lignocellulosic biomass [5, 6]. Typically, about half the starting material, most of it being lignin, ends up as solid residue after the hydrolysis step. At present it is only used as a low value fuel or soil conditioner which puts economic constraints on the process. Value addition of this residue can address this issue and improve the sustainability of 2nd generation bioethanol production [7, 8].

Thermochemical modification is one potential route for biomass valorization which can yield bio-oil for transportation applications, combustible gases for power generation, as well as other chemical intermediates [9]. In this context, pyrolysis of lignocelluloses has been extensively investigated. Pyrolysis of saw dust waste in N_2 and CO_2 atmosphere was found to release condensable compounds like carbonyls, ethers, and amines, besides non condensable gases like carbon dioxide and carbon monoxide [10]. Similarly, pyrolysis of oil palm empty fruit bunch is reported to yield pyrolysis oil containing oxygenated organics and hydrocarbons [11]. Use of catalysts, including noble metals and zeolites, can alter the composition and yields of pyrolysis products [9]. Different components

Cite this article as: Roy Ghatak, H. "Evolved Gases and Unified Kinetic Model for Low-temperature Thermal Decomposition of Rice Straw Hydrolysis Residue for Possible Value Addition", Periodica Polytechnica Chemical Engineering, 66(3), pp. 494–502, 2022. https://doi.org/10.3311/PPch.19673

of the lignocellulosic biomass fares differently during pyrolysis [12]. Phenols constitute one important product group in the pyrolysis of lignin [13], which is somewhat more resistant to thermal degradation than cellulose and hemicellulose [14].

One important variation in biomass pyrolysis is low-temperature thermal decomposition (LTTD), in which the material is thermally treated under oxygen limited atmosphere at comparatively low temperatures. In addition to the evolved volatiles, the solid residue from LTTD may be industrially important [15]. Residues from low temperature thermal decomposition of lignin shows significant changes from the parent lignin [16]. While CO_2, and CO are the major gaseous products during LTTD, the condensable portion mainly consists of organic acids, ketones, and phenolics [17]. LTTD of biomass to temperature of 300 °C resulted in solid residue with substantially increased higher heating value than the starting material [18]. Relatively mild degradation conditions during LTTD leads to the evolution of water vapour and light volatiles. While hemicellulose is fairly decomposed, the degradation of cellulose and lignin is limited [19].

Several research groups have focussed on the temperature dependence of thermal decomposition rate. One approach has been to trace the variation in activation energy with the progress of thermal decomposition using the isoconversional method [15, 20, 21]. The obtained activation energy distribution is then used for kinetic interpretation [22]. In another kinetic model the rate equations for different reactions are combined with the rate of heat transfer into the biomass particle through conduction [23]. Different kinetic models are proposed in technical literature to account for the dependence of biomass decomposition rate on residual mass fraction (RMF). Dependence of pyrolysis rate of sewage sludge on RMF in temperature range of 240–330 °C was analysed according to ten different model equations. For each equation form, the investigators found reasonable fit of experimental data with the correlation coefficient ranging from 0.952 to 0.997 [24]. n^{th} order dependence of pyrolysis rate on RMF was observed for Acetocell and Lignoboost lignins with reaction order between 1.22 and 1.27 [25]. In another study, kinetics of fast pyrolysis of alkali lignin followed either a first order or a $1/(1 - \text{RMF})$ dependence [26]. Considering the mechanistic complexity of biomass thermal decomposition, several researchers have examined combined kinetics using the Sestak Berggren empirical model [27, 28].

Most of the research on thermochemical processing of lignocelluloses has inadvertently concentrated on the whole biomass or the individual components – cellulose, hemicellulose, and lignin. In addition, these studies mainly focus on intermediate to high temperature processes, the primary target being energy products. No research finding is reported on the possible LTTD of leftover solid residue after hydrolysis of lignocelluloses. The present study is an analysis of the LTTD behaviour of the solid residue left after acid hydrolysis of rice straw to ascertain the potential of producing intermediate organic chemicals as possible replacement to petrochemicals. Attempt is also made to analyse the process kinetics and propose a uniform model.

2 Materials and methods

2.1 Materials

Rice straw used in the study was sourced from a nearby farm situated at village Longowal, Punjab, India, after the harvesting of paddy. Straw stalks were washed with water to remove external dust and dirt. Washed material was air dried in sunlight to constant mass and coarsely cut into small pieces of 1±0.2 cm. Rice straw so obtained was subjected to two stage acid hydrolysis. In the first stage 100 g (oven dry mass) of rice straw pieces was taken in a 2 L stainless steel reaction bomb. To this was added 1 L dilute H_2SO_4 solution having 3% acid based on oven dry mass of rice straw. The material was thoroughly mixed to uniformly impregnate the rice straw with the acid solution and the reaction bomb was sealed. It was then heated for 20 minutes in a preheated oven at 120 °C. The contents were cooled to room temperature and poured onto a 400 mesh stainless steel wire screen. Free liquid was squeezed out. Solid residue was washed with water several times till the washings were free of acid. The washed solid residue was subjected to a second stage of acid hydrolysis following the same procedure. However, in this stage heating was done in a preheated oven at 200 °C for 10 minutes. Rice straw hydrolysis residue (RSHR) obtained from two stage acid hydrolysis was oven dried and used in subsequent studies. Amount of RSHR obtained was gravimetrically determined to be 37.75% of the starting amount of rice straw.

Chemicals and reagents were procured from S. D. Finechem Ltd. Analytical grade chemicals were used in wet chemistry experiments. Deionised water was used for all experimental needs obtained from Millipore RiOS 5 Century Synergy water purifier. FTIR spectra were recorded using spectroscopy grade potassium bromide.

2.2 Preliminary characterization

Characterization of rice straw and RSHR is presented in Table 1. Results are the mean of experiments performed in duplicate. Klason lignin was determined using TAPPI standard test method T 222 om-11. For holocellulose determination the method of Lee et al. was used, as reported by Rabemanolontsoa and Saka [29]. In brief, 5 g of the material was reacted in an Erlenmeyer flask at 70 °C for 1 h with 1.5 g sodium chlorite dissolved in 150 mL water and acidified with 2 mL glacial acetic acid. At the end of 1 h, another dose of same reagents – sodium chlorite solution and acetic acid – were added to the contents of the flask and reaction continued for another hour. At the end of 2 h the procedure was repeated again. At the end of 3 h reaction the contents of the flask were filtered through a tared sintered glass filter. The solid residue was washed with water till free of acid and finally with 50 ml acetone. Washed residue was oven dried and gravimetrically determined as holocellulose. Obtained holocellulose was further tested for α, β, and γ cellulose according to TAPPI standard test method T 203 cm-09.

2.3 TGA-FTIR

For TGA-FTIR studies, Netzsch make TG 209 F3 Tarsus thermogravimetric analyser was coupled with the gas cell of Bruker make Tensor 27 FTIR instrument through a heated transfer line to prevent condensation of evolved species, especially water vapour. For each experiment, about 10 mg of RSHR was placed in alumina crucible and heated according to the pre-set temperature protocol. TGA was performed with heating rates of 20, 30, 40, and 50 °C/min. Inert atmosphere during TGA was maintained by nitrogen flowing at 80 mL/min. Mass loss and mass loss rate were calculated as a percentage of the initial sample mass for each TGA run. Evolved gases during TGA passed through the transfer line to enter the gas cell where FTIR spectra were recorded in real time. The transfer line and the FTIR gas cell were maintained at 250 °C. Spectra were recorded in the 4000–650 cm^{-1} range every 16 s at a spectral resolution of 4 cm^{-1} with co additions of 8 scans.

Table 1 Characterization of rice straw and RSHR

Parameters	Rice straw	RSHR
Volatile matter (%)[a]	60.6±3.7	63.8±4.2
Fixed carbon (%)[a]	21.2±1.4	20.8±1.2
Ash (%)[a]	18.2±1.0	15.4±0.9
Klason lignin (%)[a]	14.6±0.9	47.7±3.7
Holocellulose (%)[a]	67.2±4.2	36.9±2.8
α Cellulose (%)[b]	31.2±2.8	29.4±2.4
β Cellulose (%)[b]	32.5±2.2	29.8±1.9
γ Cellulose (%)[b]	36.3±2.9	40.8±3.1

[a] Values based on oven dry weight of respective materials
[b] Values based on oven dry weight of holocellulose from respective materials

3 Results and discussion

As shown in Table 1, RSHR is lignocellulosic in nature. But there is a distinct deviation from the parent rice straw. Compared to rice straw, RSHR has significantly higher amount of lignin and γ cellulose. The high amount of lignin present should have a strong bearing on its thermochemical degradation behaviour.

3.1 TGA-FTIR analysis of LTTD

3.1.1 Thermogravimetric analysis

Fig. 1 (a) represents the percentage mass loss of RSHR during heating to 350 °C at different heating rates. The initial

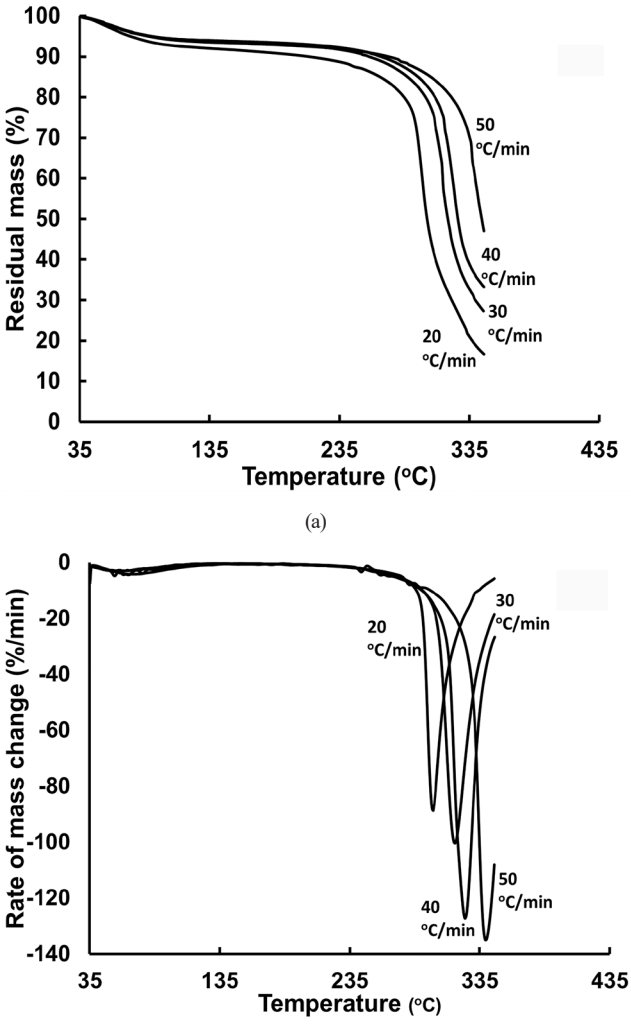

Fig. 1 TGA and DTG results of LTTD of RSHR at different heating rates, (a) TGA showing percent residual mass at different temperature, (b) DTG showing rate of mass loss at different temperature

mass loss up to a temperature of 120 °C is attributed to loss of moisture. Thereafter, up to a temperature of 250 °C the material loses very little mass, about 2% up to 200 °C at heating rate of 20 °C/min and another about 3% between 200 to 250 °C, which is mainly due to the loss of bound moisture. These values are even less at higher heating rates and account for 0.85% and 1.36%, respectively.

It is, therefore apparent that no appreciable thermal decomposition sets in in RSHR up to a temperature of 250 °C. Past 250 °C, we can observe the onset of thermal decomposition. At heating rate of 20 °C/min, material loses 32% mass between 250 and 300 °C, and another 38% between 300 and 350 °C. At heating rate of 30 °C/min, mass loss between 250 and 300 °C was 10%, and that between 300 and 350 °C was a significant 53%. When heating rate was raised to 40 °C min^{-1}, the mass loss in these temperature intervals were 8%, and 50%, respectively. At 50 °C min^{-1} heating rate, RSHR lost only 5.3% mass between 250 and 300 °C, which increased to 39% between 300 and 350 °C.

These observations are further strengthened by the differential thermogravimetry (DTG) curves shown in Fig. 1 (b). Up to a temperature of 280 °C the rate of mass loss is less than 10%/min for all heating rates. Beyond this temperature, RSHR thermally decomposes with progressively increasing rates of mass loss. At heating rate of 20 °C/min, the maximum rate of mass loss is obtained at 299 °C where the instantaneous rate of mass loss is 89%/min. With further increase in temperature the rate of mass loss keeps on decreasing which may be due to the diminishing residual mass left in the material. Similar trends were observed at increased heating rates but the occurrence of the maximum rate of mass loss shifted to progressively higher temperatures with sharper peaks as the heating rate was increased.

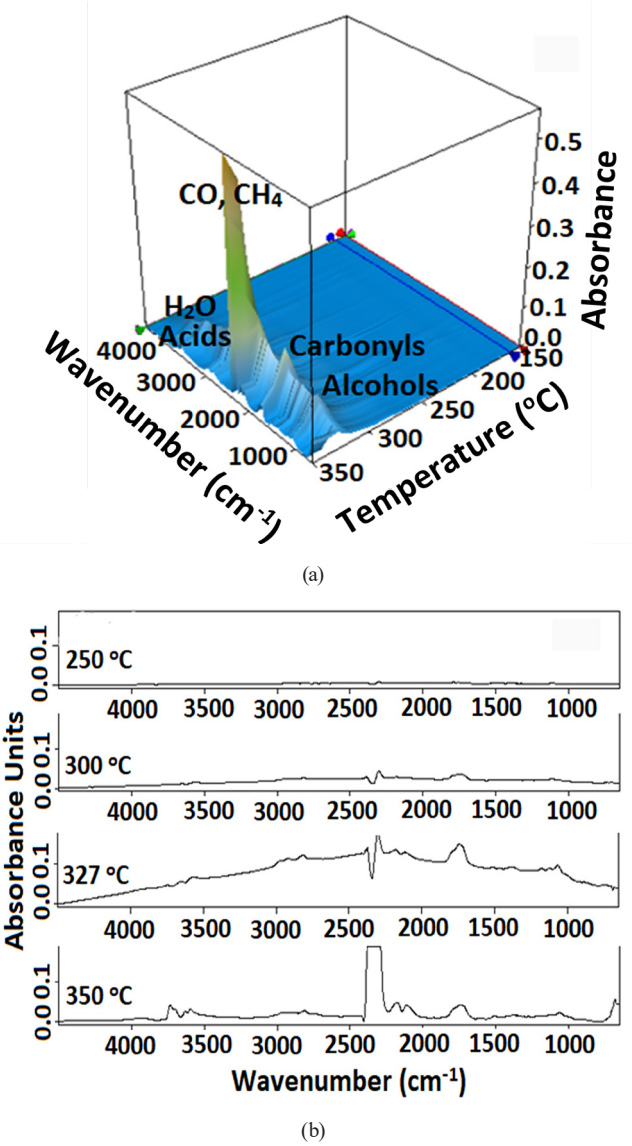

Fig. 2 FTIR spectra and temperature dependent evolution profiles of evolved gases during heating of RSHR, (a) Real time composite 3D FTIR spectra (b) Extracted spectral traces at different temperatures

3.1.2 Evolved gases analysis through FTIR spectra

Real time composite 3D FTIR spectra of the gases evolved during the heating of RSHR up to 350 °C at 50 °C min^{-1} is shown in Fig. 2 (a). The extracted FTIR spectra at temperatures 250 °C, 300 °C, 350 °C, and 327 °C are shown in Fig. 2 (b). It is clearly visible that the absorption bands are insignificant in the FTIR spectra recorded up to a temperature of about 250 °C which conforms to the mass loss behaviour observed during TGA. Feeble absorption bands which did appear between 200 and 250 °C are cluster between 3900–3550 cm^{-1} (major peaks 3866, 3730, and 3553 cm^{-1}), 2347 cm^{-1}, and a pair of peaks at 1790 and 1752 cm^{-1}. These may be assigned to O–H stretching in H_2O and low molecular mass carboxylic acids [17], C=O stretching in CO_2, and C=O stretching in carbonyls of acids, respectively [9, 30, 31]. In the temperature interval of 250 to 300 °C, which accounts for 5.29% mass loss, the major absorption bands appearing in the FTIR spectra are cluster between 3900–3550 cm^{-1} (major peaks 3739, 3648, and 3555 cm^{-1}), 2929 cm^{-1}, 2347 cm^{-1}, 2181 cm^{-1}, 2117 cm^{-1}, 1752 cm^{-1}, and 1514 cm^{-1}. Of these, the 3900–3550 cm^{-1} cluster of bands arise from O–H stretching in H_2O, low molecular mass carboxylic acids, and methanol [17]. The bands at 2929 cm^{-1}, and 2181 cm^{-1}, are due to C–H symmetric stretching in CH_4, and C–O stretching in CO, respectively [32]. The carbonyl stretch at 1790 cm^{-1} only appears as a shoulder indicating some decarboxylation. 1514 cm^{-1} band arises from skeletal stretching in aromatic ring. 1378 cm^{-1} band is assigned to C–H symmetric bending in methyl groups of acetic acid and methanol [17].

There is a marked increase in the evolution of gaseous products beyond 300 °C as noticed in the sharp increase in absorption band intensities in the FTIR spectra. Besides the bands for H_2O, CO_2, CO, CH_4, other non-methane hydrocarbons, carboxylic acids, and aromatic carbonyls, additional bands are observed in the FTIR spectra. The band at 1363 cm^{-1} is assigned to C–C and C–H stretching of alkanes, whereas the band at 1055 cm^{-1} is owing to C–O stretching from the formation of alcohols and phenols [32]. There is also a shoulder centred at 1378 cm^{-1}. It is, however, interesting to note the shift in carbonyl peaks to lower wavenumbers as the decomposition temperature is increased. At 250 °C it appears at 1790 cm^{-1} which is most likely due to phenyl esters. At 300 °C the carbonyl peak is at 1752 cm^{-1}. At 327 °C it appears at 1741 cm^{-1} and at 350 °C it further shifts to 1735 cm^{-1} which indicates the presence of aldehydes or ketones.

3.2 LTTD kinetics of RSHR using thermogravimetry

3.2.1 Activation energy of LTTD

The rate of a chemical reaction depends on the temperature and composition of the reacting system [33], which, in general terms, may be represented as

$$\text{Rate} = f\left(T, \text{composition}\right). \tag{1}$$

For single reactions, it is adequate to transform the Eq. (1) as

$$\text{Rate} = f_1\left(T\right) f_2\left(\text{composition}\right), \tag{2}$$

where f_1 is a function independent of composition, and f_2 is a function independent of temperature. Thus, at given composition of the reacting system, f_2(composition) may be taken as a constant, and Eq. (2) reduces to

$$\text{Rate} = A f_1\left(T\right). \tag{3}$$

Similarly, at a given temperature, $f_1(T)$ may be taken as a constant, and Eq. (2) reduces to

$$\text{Rate} = B f_2\left(\text{composition}\right), \tag{4}$$

where A, and B are constants at given composition and temperature, respectively. In majority of cases the function $f_1(T)$ follows the well known Arrhenius equation.

Attempts have been made to adopt a similar approach for the kinetic interpretation of biomass thermal decomposition process [20] with the rate being expressed as

$$-\frac{d\left(\text{RMF}\right)}{dt} = f_1\left(T\right) f_2\left(\text{RMF}\right), \tag{5}$$

where RMF is the residual mass fraction, t is decomposition time, and T is the absolute temperature.

If the temperature dependence of decomposition rates follows the Arrhenius equation, Eq. (5) would transform to

$$-\frac{d\left(\text{RMF}\right)}{dt} = A\exp\left\{\frac{-E_a\left(\text{RMF}\right)}{RT}\right\} f_2\left(\text{RMF}\right), \tag{6}$$

where A is the pre exponential factor, and R is the universal gas constant. The term E_a(RMF) is the activation energy dependent on RMF, according to the Distributed Activation Energy Model (DAEM) [34]. This model accounts for the fact that thermal decomposition of biomass components is a complex process, which involves several reaction steps intricately joined through series as well as parallel combinations. The measured activation energy for the thermochemical decomposition as a whole is, in fact, the cumulative weighted average of the different activation energies of all the contributing reaction steps. Further, the individual contribution of each of these steps follows a continuous distribution over the entire range of RMF. As a result, the measured activation energy for the thermochemical decomposition as a whole should vary with RMF and follow a continuous distribution over the entire range of RMF.

For evaluating the activation energy at different RMF, the differential method of analysis using the isoconversional approximation was used [35]. At each RMF, experimental rates at different temperatures were regressed into Eq. (6) using nonlinear least square fitting. The results are shown in Fig. 3 (a) and (b). This allowed for the computation of activation energies at different RMF and the distribution of activation energies is shown in Fig. 3 (c). Through nonlinear regression, the distribution of activation energies fits well into a Lorentzian distribution with a coefficient of determination, R^2, of 0.945 and Adj. R^2 of 0.932. Variation of activation energies for thermal decomposition of RSHR over varying RMF may be expressed as

$$E_a\left(\text{RMF}\right) = \frac{159.8982}{1+\left(\frac{\text{RMF}-0.7524}{0.0779}\right)^2}. \tag{7}$$

3.2.2 Rate dependence on residual mass fraction

Model fitting through nonlinear regression was used to determine the form of the function f_2(RMF) in Eq. (6). Considering the complexity of the decomposition process, phase transformations, mass transfer, and chemical transformation are all involved. Attempts have been made to

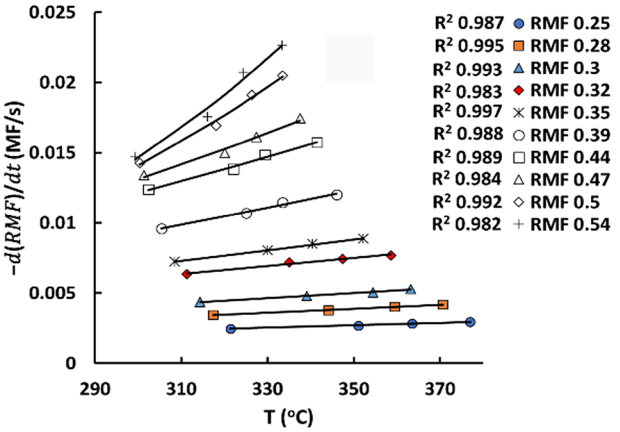

(a)

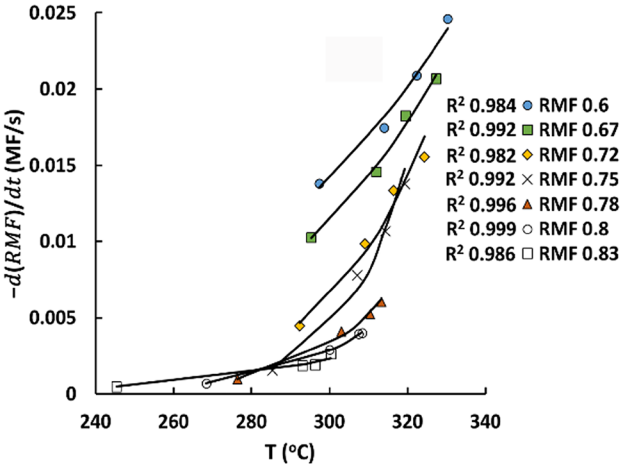

(b)

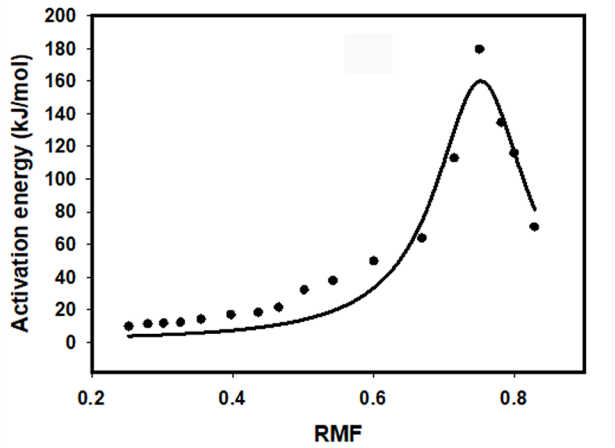

(c)

Fig. 3 Activation energies of LTTD of RSHR by isoconversional differential method, (a) computation by nonlinear least squares fitting to Eq. (6), RMF 0.25–0.54; (b) computation by nonlinear least squares fitting to Eq. (6), RMF 0.6–0.83; (c) Lorentzian distribution of activation energies over varying RMF. In all figures, solid lines represent regressed equations and markers represent experimentally determined values.

model the decomposition process based on the predominance of one or the other mechanism [21]. In kinetics parlance, it is often useful to express the reaction rate to be proportional to RMF raised to an exponent n; n being termed as the order. But in the present case, the rate data could not be satisfactorily fitted into a reaction model following n^{th} order kinetics. Next, model fitting of rate data was done to different diffusional models as well as Avrami–Erofeev models [21]. But in every case the data did not give a satisfactory fit.

The extent of correlation of regressed equation with the experimental rates is shown in Table 2.

Obviously, the coefficients of determination are abysmally low indicating lack of fit. It points to the fact that thermal decomposition of RSHR is neither a one step process nor is it a process controlled by one or the other

Table 2 Coefficients of determination for regression of experimental rate data into different model equations

f_2(RMF)	Heating rate	R^2	Adj. R^2
Avrami Erofeev $4(RMF)[-\ln(RMF)]^{3/4}$	20 °C/min	0.241	0.224
	30 °C/min	0.402	0.39
	40 °C/min	0.387	0.375
	50 °C/min	0.36	0.346
Avrami Erofeev $3(RMF)[-\ln(RMF)]^{2/3}$	20 °C/min	0.221	0.203
	30 °C/min	0.332	0.318
	40 °C/min	0.321	0.307
	50 °C/min	0.294	0.28
Avrami Erofeev $2(RMF)[-\ln(RMF)]^{1/2}$	20 °C/min	0.134	0.115
	30 °C/min	0.168	0.151
	40 °C/min	0.174	0.157
	50 °C/min	0.162	0.145
n^{th} order $0.0023(RMF)^{-0.86}$	20 °C/min	–0.16	–0.185
	30 °C/min	0.19	0.173
	40 °C/min	0.17	0.153
	50 °C/min	0.131	0.113
3 dimensional diffusion $3/2(RMF)^{2/3}[1-(RMF)^{1/3}]^{-1}$	20 °C/min	0.0984	0.0782
	30 °C/min	0.5	0.49
	40 °C/min	0.5	0.49
	50 °C/min	0.499	0.489
2 dimensional diffusion $[-\ln(RMF)]^{-1}$	20 °C/min	–0.692	–0.73
	30 °C/min	–0.33	–0.357
	40 °C/min	–0.287	–0.314
	50 °C/min	–0.224	–0.249
1 dimensional diffusion $1/2[1-(RMF)]^{-1}$	20 °C/min	–0.657	–0.694
	30 °C/min	–0.321	–0.348
	40 °C/min	–0.28	–0.306
	50 °C/min	–0.218	–0.243

mechanistic steps. To find the dependence of decomposition rate on RMF the empirical rate equation of truncated Sestak and Berggren model [21, 27, 28] was fitted into the experimental rate data under different decomposition conditions. The resultant kinetic equation, with the following general form, fits well into the experimental data:

$$-\frac{d(\mathrm{RMF})}{dt} = A\exp\left\{\frac{-E_a(\mathrm{RMF})}{RT}\right\}(1-\mathrm{RMF})^m(\mathrm{RMF})^n, \quad (8)$$

where E_a(RMF) is following Eq. (7). Dependence of reaction rate on RMF is expected and self-explanatory. The quantity (1 − RMF) at any instance represents the fraction of material lost as a result of thermal decomposition. This fraction is made up of the gaseous products of LTTD. As gases are produced and make their way through the residual solid mass, the internal structure of the solid offers a resistance to their escape. At the same time, the escaping gases have a bearing on the morphological character of the solid left behind. As thermal decomposition progresses, the residual solid mass gradually increases in void fraction. The increased porosity facilitates the escape of gases. This explains the positive influence of the quantity (1 − RMF) on decomposition rate.

Model parameters are given in Table 3. Results for thermal decomposition of RSHR under different heating rates are shown in Fig. 4. The coefficients of determination, as measured by R^2, is sufficiently high which shows that most of the variations in decomposition rates can be accurately correlated to the variations in temperature, activation energy, and RMF by the proposed model. Close correspondence between the values of R^2 and Adj. R^2 further points to the unbiased statistical significance of the model. A single rate equation that could cater to all the heating rates should be preferred because of better adaptability in equipment design. Report on LTTD kinetics of RSHR is not available in technical literature. For closest comparison the exponents *m*, and *n* are reported to be 1.8428, and 1.1816, respectively for TGA of mixed agricultural residue up to 800 °C [28]. In another study, the values for *m*, and *n* for the pyrolysis of lignin varied in different mass fraction ranges. In 0.8–0.9 range of RMF exponent *m* was 2.718

Table 3 Parameters for kinetic equations from DAEM with truncated Sestak and Berggren model

Heating rate	*A*	*m*	*n*	R^2	Adj. R^2
20 °C/min	40.7904	4.8067	6.3264	0.934	0.933
30 °C/min	40.7904	4.8067	6.3264	0.975	0.975
40 °C/min	40.7904	4.8067	6.3264	0.981	0.980
50 °C/min	40.7904	4.8067	6.3264	0.972	0.972

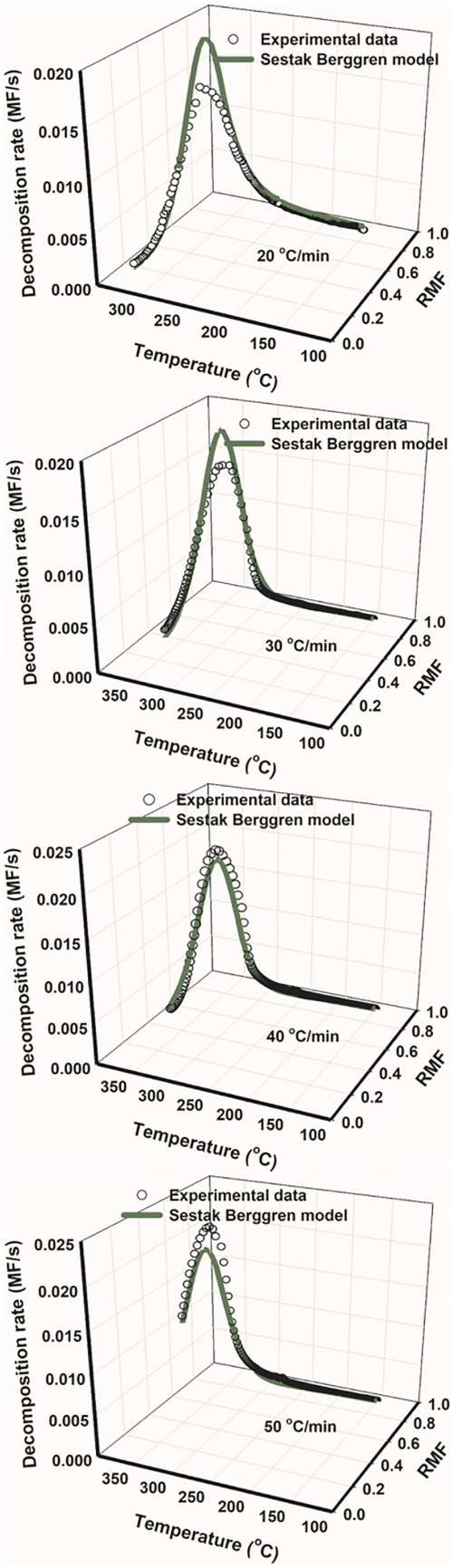

Fig. 4 Kinetic equations from DAEM with Sestak and Berggren model [Eq. (8)] fitted to experimental data for LTTD of RSHR at different heating rates

and the exponent n was 1.077. The values were 4.61 and 5.022, respectively, for RMF between 0.25–0.45 [27].

4 Conclusion

LTTD of RSHR under inert nitrogen atmosphere does not cause appreciable mass loss up to a temperature of 250 °C. Thermal decomposition mainly sets in beyond this temperature and rapid mass loss is observed above 280 °C. RSHR is devolatilized between 60 to 85% by thermally decomposing it up to a temperature of 350 °C. The maximum rate of mass loss is obtained at progressively higher temperatures as the heating rate is increased.

From the standpoint of value addition, LTTD of RSHR could yield volatile oxygenated organics including acids, esters, aldehydes, and ketones, besides alcohols and phenols. All these are industrially significant and potential replacement for petrochemicals. With increase in decomposition temperature, the extent of conjugation decreased in the carbonyl moieties. The main gaseous products of LTTD were carbon dioxide, carbon monoxide, and methane.

Rate of LTTD of RSHR could be represented as a unified kinetic model – a single equation faithfully predicting the experimental rates of thermal decomposition for all variation in RMF, temperature, and heating rate. Temperature dependence of LTTD of RSHR followed the DAEM with activation energies distributed across RMF according to Lorentzian distribution. Dependence of experimental decomposition rates on RMF could be modelled as following truncated Sestak Berggren equation. Both RMF and (1 − RMF) positively influence the rate of LTTD.

References

[1] Kumar, P., Joshi, L. "Pollution Caused by Agricultural Waste Burning and Possible Alternate Uses of Crop Stubble: A Case Study of Punjab", In: Nautiyal, S., Rao, K., Kaechele, H., Raju, K., Schaldach, R. (eds.) Knowledge Systems of Societies for Adaptation and Mitigation of Impacts of Climate Change, Springer, Berlin, Germany, 2013, pp. 367–385. https://doi.org/10.1007/978-3-642-36143-2_22

[2] Borah, N., Barua, R., Nath, D., Hazarika, K., Phukon, A., Goswami, K., Barua, D. C. "Low Energy Rice Stubble Management through in Situ Decomposition", Procedia Environmental Sciences, 35, pp. 771–780, 2016. https://doi.org/10.1016/j.proenv.2016.07.092

[3] Ministry of Environment, Forest and Climate Change, Government of India "India's Intended Nationally Determined Contribution: Working towards Climate Justice", [pdf] Ministry of Environment, Forest and Climate Change, Government of India, New Delhi, India, Available at: https://www4.unfccc.int/sites/ndcstaging/PublishedDocuments/India%20First/INDIA%20INDC%20TO%20UNFCCC.pdf [Accessed: 21 March 2020]

[4] Ministry of New & Renewable Energy, Government of India "National Policy on Biofuels", [pdf] Ministry of New & Renewable Energy, Government of India, New Delhi, India, Available at: http://164.100.94.214/sites/default/files/uploads/biofuel_policy_0.pdf [Accessed: 11 March 2020]

[5] Taherzadeh, M. J., Karimi, K. "Acid-based hydrolysis processes for ethanol from lignocellulosic materials: a review", BioResources, 2(3), pp. 472–499, 2007.

[6] Wang, C., Duan, X., Wang, W., Li, Z., Qin, Y. "Establishment and verification of a shrinking core model for dilute acid hydrolysis of lignocellulose", Frontiers in Energy, 6(4), pp. 413–419, 2012. https://doi.org/10.1007/s11708-012-0212-z

[7] Chandel, A. K., Garlapati, V. K., Singh, A. K., Antunes, F. A. F., da Silva, S. S. "The path forward for lignocellulose biorefineries: Bottlenecks, solutions, and perspective on commercialization", Bioresource Technology, 264, pp. 370–381, 2018. https://doi.org/10.1016/j.biortech.2018.06.004

[8] Zhang, Y. H. P. "Reviving the carbohydrate economy via multi-product lignocellulose biorefineries", Journal of Industrial Microbiology and Biotechnology, 35(5), pp. 367–375, 2008. https://doi.org/10.1007/s10295-007-0293-6

[9] Lazdovica, K., Liepina, L., Kampars, V. "Comparative wheat straw catalytic pyrolysis in the presence of zeolites, Pt/C, and Pd/C by using TGA-FTIR method", Fuel Processing Technology, 138, pp. 645–653, 2015. https://doi.org/10.1016/j.fuproc.2015.07.005

[10] Tang, Y., Ma, X., Wang, Z., Wu, Z., Yu, Q. "A study of the thermal degradation of six typical municipal waste components in CO_2 and N_2 atmospheres using TGA-FTIR", Thermochimica Acta, 657, pp. 12–19, 2017. https://doi.org/10.1016/j.tca.2017.09.009

[11] Kusworo, T. D., Widayat, W., Mahadita, A. F., Firizqina, D., Utomo, D. P. "Bio-oil and Fuel Gas Production from Agricultural Waste via Pyrolysis: A Comparative Study of Oil Palm Empty Fruit Bunches (OPEFB) and Rice Husk", Periodica Polytechnica Chemical Engineering, 64(2), pp. 179–191, 2020. https://doi.org/10.3311/PPch.14553

[12] Yang, H., Yan, R., Chen, H., Lee, D. H., Zheng, C. "Characteristics of hemicellulose, cellulose and lignin pyrolysis", Fuel, 86(12–13), pp. 1781–1788, 2007. https://doi.org/10.1016/j.fuel.2006.12.013

[13] Hatakeyama, H., Tsujimoto, Y., Zarubin, M. J., Krutov, S. M., Hatakeyama, T. "Thermal decomposition and glass transition of industrial hydrolysis lignin", Journal of Thermal Analysis and Calorimetry, 101, pp. 289–295, 2010. https://doi.org/10.1007/s10973-010-0698-8

[14] Chen, T., Li, L., Zhao, R., Wu, J. "Pyrolysis kinetic analysis of the three pseudocomponents of biomass–cellulose, hemicellulose and lignin", Journal of Thermal Analysis and Calorimetry, 128, pp. 1825–1832, 2017. https://doi.org/10.1007/s10973-016-6040-3

[15] Chen, D., Gao, A., Cen, K., Zhang, J., Cao, X., Ma, Z. "Investigation of biomass torrefaction based on three major components: Hemicellulose, cellulose, and lignin", Energy Conversion and Management, 169, pp. 228–237, 2018. https://doi.org/10.1016/j.enconman.2018.05.063

[16] Reddy, I. A. K., Ghatak, H. R. "Low-temperature thermal degradation behaviour of non-wood soda lignins and spectroscopic analysis of residues", Journal of Thermal Analysis and Calorimetry, 132, pp. 407–423, 2018. https://doi.org/10.1007/s10973-017-6912-1

[17] Lv, P., Almeida, G., Perré, P. "TGA-FTIR analysis of torrefaction of lignocellulosic components (cellulose, xylan, lignin) in isothermal conditions over a wide range of time durations", BioResources, 10(3), pp. 4239–4251, 2015.

[18] Da Silva, J. C. G., Pereira, J. L. C., Andersen, S. L. F., Moreira, R. F. P., Jose, H. J. "Torrefaction of ponkan peel waste in tubular fixed-bed reactor: In-depth bioenergetic evaluation of torrefaction products", Energy, 210, Article number: 118569, 2020. https://doi.org/10.1016/j.energy.2020.118569

[19] Dai, L., Wang, Y., Liu, Y., Ruan, R., He, C., Yua, Z., Jiang, L., Zeng, Z., Tian, X. "Integrated process of lignocellulosic biomass torrefaction and pyrolysis for upgrading bio-oil production: A state-of-the-art review", Renewable and Sustainable Energy Reviews, 107, pp. 20–36, 2019. https://doi.org/10.1016/j.rser.2019.02.015

[20] Martín-Lara, M. A., Blázquez, G., Zamora, M. C., Calero, M. "Kinetic modelling of torrefaction of olive tree pruning", Applied Thermal Engineering, 113, pp. 1410–1418, 2017. https://doi.org/10.1016/j.applthermaleng.2016.11.147

[21] Baroni, E. G., Tannous, K., Rueda-Ordóñez, Y. J., Tinoco-Navarro, L. K. "The applicability of isoconversional models in estimating the kinetic parameters of biomass pyrolysis", Journal of Thermal Analysis and Calorimetry, 123, pp. 909–917, 2016. https://doi.org/10.1007/s10973-015-4707-9

[22] Rego, F., Dias, A. P. S., Casquilho, M., Rosa, F. C., Rodrigues, A. "Pyrolysis kinetics of short rotation coppice poplar biomass", Energy, 207, Article number: 118191, 2020. https://doi.org/10.1016/j.energy.2020.118191

[23] Miljković, B., Nikolovski, B., Mitrović, D., Janevski, J. "Modeling for Pyrolysis of Solid Biomass", Periodica Polytechnica Chemical Engineering, 64(2), pp. 192–204, 2020. https://doi.org/10.3311/PPch.14039

[24] Naqvi, S. R., Tariq, R., Hameed, Z., Ali, I., Naqvi, M., Chen, W.-H., Ceylan, S., Rashid, H., Ahmad, J., Taqvi, S. A., Shahbaz, M. "Pyrolysis of high ash sewage sludge: Kinetics and thermodynamic analysis using Coats-Redfern method", Renewable Energy, 131, pp. 854–860, 2019. https://doi.org/10.1016/j.renene.2018.07.094

[25] Janković, B. "The comparative kinetic analysis of Acetocell and Lignoboost® lignin pyrolysis: The estimation of the distributed reactivity models", Bioresource Technology, 102(20), pp. 9763–9771, 2011. https://doi.org/10.1016/j.biortech.2011.07.080

[26] Ojha, D. K., Viju, D., Vinu, R. "Fast pyrolysis kinetics of alkali lignin: Evaluation of apparent rate parameters and product time evolution", Bioresource Technology, 241, pp. 142–151, 2017. https://doi.org/10.1016/j.biortech.2017.05.084

[27] Yeo, J. Y., Chin, B. L. F., Tan, J. K., Loh, Y. S. "Comparative studies on the pyrolysis of cellulose, hemicellulose, and lignin based on combined kinetics", Journal of the Energy Institute, 92(1), pp. 27–37, 2019. https://doi.org/10.1016/j.joei.2017.12.003

[28] Wang, X., Hu, M., Hu, W., Chen, Z., Liu, S., Hu, Z., Xiao, B. "Thermogravimetric kinetic study of agricultural residue biomass pyrolysis based on combined kinetics", Bioresource Technology, 219, pp. 510–520, 2016. https://doi.org/10.1016/j.biortech.2016.07.136

[29] Rabemanolontsoa, H., Saka, S. "Holocellulose Determination in Biomass", In: Yao, T. (ed.) Zero-Carbon Energy Kyoto 2011, Springer, Tokyo, Japan, 2012, pp. 135–140. https://doi.org/10.1007/978-4-431-54067-0_14

[30] Ma, Z., Chen, D., Gu, J., Bao, B., Zhang, Q. "Determination of pyrolysis characteristics and kinetics of palm kernel shell using TGA–FTIR and model-free integral methods", Energy Conversion and Management, 89, pp. 251–259, 2015. https://doi.org/10.1016/j.enconman.2014.09.074

[31] Yuzbasi, N. S., Selçuk, N. "Air and oxy-fuel combustion characteristics of biomass/lignite blends in TGA-FTIR", Fuel Processing Technology, 92(5), pp. 1101–1108, 2011. https://doi.org/10.1016/j.fuproc.2011.01.005

[32] Cao, X., Zhong, L., Peng, X., Sun, S., Li, S., Liu, S., Sun, R. "Comparative study of the pyrolysis of lignocellulose and its major components: Characterization and overall distribution of their biochars and volatiles", Bioresource Technology, 155, pp. 21–27, 2014. https://doi.org/10.1016/j.biortech.2013.12.006

[33] Ghatak, H. R. "Reaction Engineering Principles", CRC Press, Boca Raton, FL, USA, 2016, pp. 29–36. https://doi.org/10.1201/9781315367781

[34] Navarro, M. V., Murillo, R., Mastral, A. M., Puy, N., Bartroli, J. "Application of the Distributed Activation Energy Model to Biomass and Biomass Constituents Devolatilization", AIChE Journal, 55(10), pp. 2700–2715, 2009. https://doi.org/10.1002/aic.11848

[35] Bardow, A., Marquardt, W. "Incremental and simultaneous identification of reaction kinetics: methods and comparison", Chemical Engineering Science, 59(13), pp. 2673–2684, 2004. https://doi.org/10.1016/j.ces.2004.03.023